Computational Materials Science 77 (2013) 145–152

Contents lists available at SciVerse ScienceDirect

Computational Materials Science

journal homepage: www.elsevier.com/locate/commatsci

Conversion of optically isotropic to anisotropic CdS_xSe_{1-x} $(0 \leqslant x \leqslant 1)$ alloy with S concentration

Imad Khan [a,*], Iftikhar Ahmad [a], H.A. Rahnamaye Aliabad [b], S. Jalali Asadabadi [c], Zahid Ali [a], M. Maqbool [d]

[a] Department of Physics, University of Malakand, Chakdara, Pakistan
[b] Department of Physics, Hakim Sabzevary University, Sabzevar, Iran
[c] Department of Physics, University of Isfahan, Hezar Gerib Avenue, Isfahan 81744, Iran
[d] Department of Physics and Astronomy, Ball State University, Muncie, IN 47306, USA

ARTICLE INFO

Article history:
Received 18 December 2012
Received in revised form 1 April 2013
Accepted 15 April 2013

Keywords:
Anisotropy
Semiconductors
Electronic band structure
Birefringence

ABSTRACT

Structural, electronic and optical properties of CdS_xSe_{1-x} at various compositions $(0 \leqslant x \leqslant 1)$ are investigated using full potential linearized augmented plane waves (FP-LAPWs) method. A structural phase transition from zinc-blende to wurtzite is observed in CdS_xSe_{1-x} with increase in S concentration. The theoretically calculated phase transition as well as structural parameters like ground state energies, lattice constants and bulk moduli is in agreement with the experimental results. As CdS_xSe_{1-x} compound belongs to strongly correlated systems, therefore modified Becke–Johnson potential is used to calculate band gap energies and optical properties of the compound. The direct band gap nature of the material varies in the visible part of the spectral region for the whole range of S. The optical properties, like dielectric functions, refractive index, birefringence and energy loss function, are also calculated. The hexagonal wurtzite CdSSe is anisotropic and the calculated birefringence is found to be positive in the lower energy levels and negative in the higher levels.

1. Introduction

The zinc, cadmium and mercury (Zn, Cd, Hg) oxides and chalcogenides are promising materials for optoelectronic devices such as LED's, lasers, sensors, detectors and solar cells. The band gap energies of these compounds cover the full range of electromagnetic spectrum i.e. from infrared (IR) to ultraviolet (UV). Because of their wide range of band gap energies, simple and easy synthesis and flexibility for both p and n type doping, they are very attractive in optoelectronic industry. These materials are extensively studied in the last two decades due to their important properties [1–3]. The strong p–d coupling between the II^B and chalcogen elements make them strongly correlated systems [4]. The earlier potentials of density functional theory (DFT) like local density approximation (LDA), generalized gradient approximation (GGA), GW and LDA + U were not successful in appropriate description of the strongly correlated p–d coupling in these compounds, which resulted in severe underestimation of band gaps and other physical properties [5]. The recent theoretical research on II–VI semiconductors [6–11] shows that the modified Becke–Johnson potential has efficiently solved this problem.

CdSSe has many established applications in optoelectronic devices operating in the visible region of the electromagnetic spectrum such as LED's, sensors, solar cells, filters, and non-linear optical communications [12–18]. The binary semiconductors CdS and CdSe crystallize in either hexagonal wurtzite or cubic zinc-blende phase. The investigation of their ternary alloys is interesting from the band gap engineering point of view, because both exhibit band gaps in the visible region. Similar work for $Cd_{1-x}Zn_xS$ [4] and for $Ga_{1-x}Zn_xN_{1-x}O_x$ [5,19] also enlightens the importance of the materials that works in the visible ranges.

CdSSe can be synthesized in bulk and nanostructures. Agnihotri and Raturi [20] grown CdS_xSe_{1-x} film by using pyrolytic decomposition techniques and found predominant hexagonal structure. Kumar and Sharma [21] fabricated thin film of CdS_xSe_{1-x} by using screen printing method and found zinc-blende structure for $x < 0.4$ and wurtzite for $x > 0.4$. White et al. [22] reported nanocrystal of CdS_xSe_{1-x} by sequential ion implantation and annealing, obtained hexagonal wurtzite structure in SiO_2 and Al_2O_3, and cubic zinc-blende structure in Si. Pan et al. [23] have grown CdSSe nanowires and nanoribbons by thermal evaporation route and obtained wurtzite structure for $CdS_{0.6}Se_{0.4}$ and $CdS_{0.3}Se_{0.7}$ nanowires and nanoribbons respectively. Kainthla et al. [24] prepared thin films of CdS_xSe_{1-x} and found cubic zinc-blende structure by using electron diffraction analysis. Liang et al. [25] reported the fabrication

* Corresponding author. Tel.: +92 344 6643723.
E-mail address: Imadkhan723@gmail.com (I. Khan).

0927-0256/$ - see front matter © 2013 Elsevier B.V. All rights reserved.
http://dx.doi.org/10.1016/j.commatsci.2013.04.030

of CdSSe nanowires through a template assisted electrodeposition method. CdSSe nanostructures were grown using physical vapor transport method by Kim et al. [26] and obtained wurtzite crystallographic structures. Liu et al. [27] have grown polycrystalline of CdSSe nanowires in wurtzite with a low temperature by physical evaporation method. Ouendadji et al. [28] studied the structural, electronic, optical and thermodynamic properties of CdSSe in the zinc-blende phase using density functional theory but the results are not consistent with the experiments and hence need to be revisited with a more reliable theoretical model, so that the results may be comparable to experimental results. Keeping in view this important aspect and wide practical applications of the CdSSe in the optoelectronic industry, modified Becke–Johnson potential ensemble with generalized gradient approximation (GGA) is used to investigate structural, electronic and optical properties of CdS_xSe_{1-x}.

2. Computational details

In the present study CdS_xSe_{1-x} is modeled at various compositions with a step of 0.25 using eight atoms per unit cell, for both zinc-blende and wurtzite phases. The full potential linearized augmented plane waves (FP-LAPWs) method as implemented in the WIEN2k package [29] is used to calculate the structural, electronic and optical properties of CdS_xSe_{1-x} $(0 \leqslant x \leqslant 1)$. The generalized gradient approximation (GGA) is used for the structural properties and the modified Becke–Johnson (mBJ) exchange potential is used for the electronic and optical properties [6]. In the full potential scheme, the potential and charge density are expanded by spherical harmonics inside the non-overlapping spheres (muffin-tin spheres) and by plane wave basis set in the remaining space of the unit cell (interstitial region). For the wave function expansion inside the atomic spheres, the value of l is confined to $l_{max} = 10$, and for the interstitial non-spherical part $l_{max} = 6$. The muffin-tin radii for Cd, S and Se are selected in such way that no charge leakage from the core is taken place and the total energy is converged. For the wave function in the interstitial region the plane wave cut-off value of K_{max} is $8/R_{MT}$, while the charge density is Fourier expanded up to $G_{max} = 14$ (Ry). The brillouin zone integration is performed using a mesh of 2000 k-points, and convergence is checked through self-consistency. The ideal internal parameter $u = 0.375$ for the wurtzite structures is used, while c/a is optimized.

3. Structural properties

A partial substitution of an element by another element in a compound can cause drastic changes in physical properties of parent material. In the present work CdSe is assumed as a parent material and Se is partially substituted by S. The total energy for each concentration is calculated and it is found that CdSe is more stable in the zinc-blende structure while CdS prefers wurtzite phase, which is an agreement with the earlier reported theoretical results [30]. The mixed ternary alloy of CdSe and CdS crystallizes in either zinc-blende or wurtzite phase, depending upon the concentration of S. The partial substitution of S in CdSe at a particular concentration changes the crystal phase from zinc-blende to wurtzite, which is also observed in experiments [21,22].

Each alloy of CdS_xSe_{1-x} $(0 \leqslant x \leqslant 1)$ is modeled in the steps of 0.25 in both zinc-blende and wurtzite crystal structures, and each unit cell is optimized by minimizing the total energy with respect to the cell volume. The calculated lattice constants and bulk moduli are obtained by fitting the total energy versus unit cell volume to the Murnaghan's equation of state [31]. The optimization curves (total energy as a function of lattice volume) for both of these phases at different concentrations are presented in Fig. 1. It is obvious from the figure that the normal phase of $CdS_{0.25}Se_{0.75}$ and $CdS_{0.50}Se_{0.50}$ is zinc-blende, while at $x = 0.75$ the stable phase of the compound is wurtzite. The ground state energy as a function of concentration for ternary alloys in the zinc-blende as well as wurtzite phases are shown in Fig. 2. It is clear from the figure that as the concentration of S in CdSSe is increased from $x = 0.25$ to 0.50 the energy difference between the two phases is reduced, while on further increase in S concentration (75%) the energy difference becomes negligible with a smaller value for the wurtzite phase. In

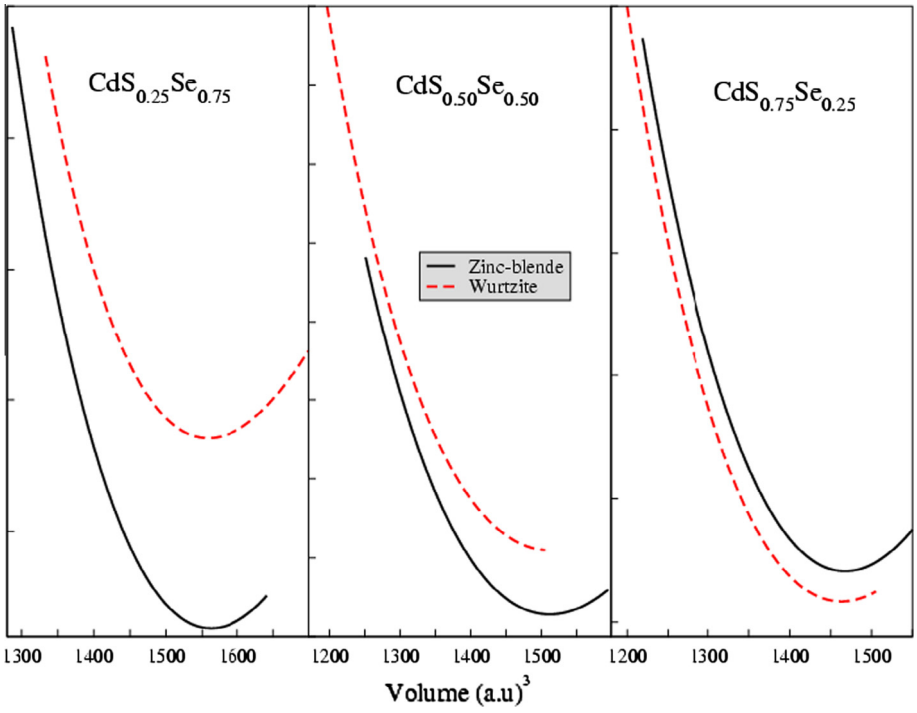

Fig. 1. Variation of total energy as a function of unit cell volume of $CdS_{0.25}Se_{0.75}$, $CdS_{0.50}Se_{0.50}S$ and $CdS_{0.75}Se_{0.25}$.

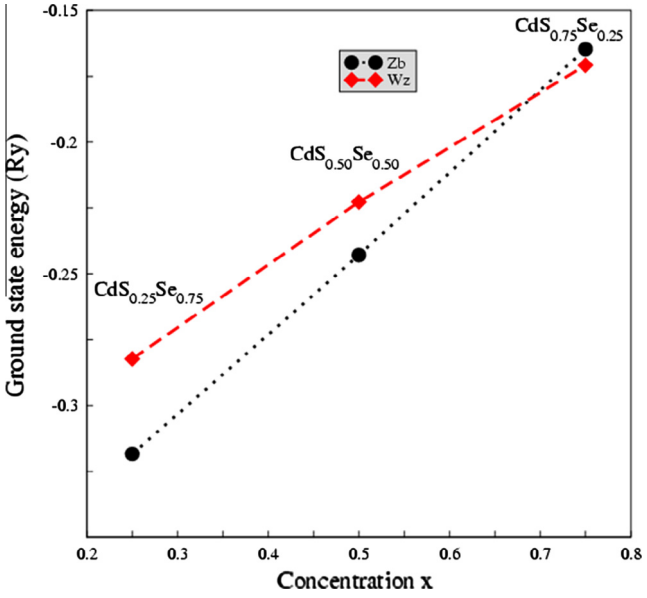

Fig. 2. Total ground state energies of $CdS_{0.25}Se_{0.75}$, $CdS_{0.50}Se_{0.50}$, and $CdS_{0.75}Se_{0.25}$ in the zinc-blende and wurtzite phases.

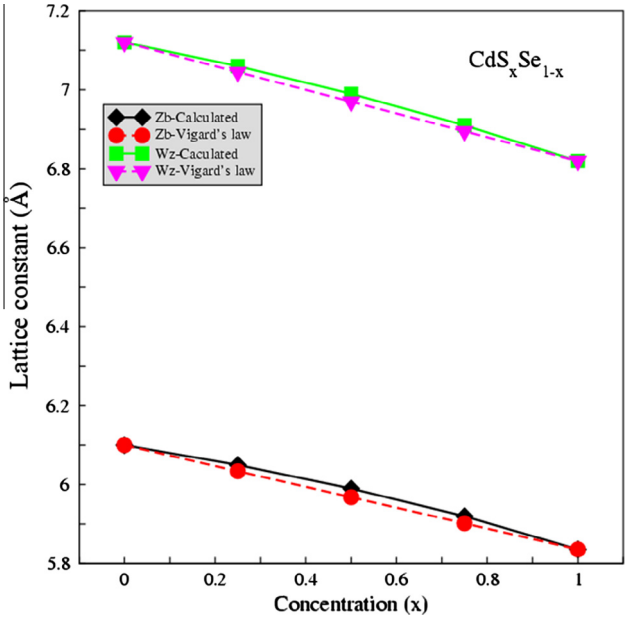

Fig. 3. Variation of lattice constants of $CdS_{0.25}Se_{0.75}$, $CdS_{0.50}Se_{0.50}$, and $CdS_{0.75}Se_{0.25}$ in the zinc-blende and wurtzite phases.

fact at $x = 0.75$, the wurtzite phase is more stable than that of the zinc-blende phase, viz., $E_{WZ} - E_{ZB} < 0$, whereas the later phase is more stable than the former one at $x = 0.25$ and $x = 0.5$, viz., $E_{ZB} - E_{WZ} < 0$. Thus, the crystal phase transforms from the zinc-blende to wurtzite within the range $x = 0.50-0.75$. From the interpolation of Fig. 2, the phase transition is obtained at 68% of S concentration. As the energy difference between the two phases is very small (see Table 1), so it is possible that the phase transition can be observed earlier or later than the 68% of the S concentration, depending upon the external pressure and other physical parameters.

The structural parameters like lattice constants and bulk moduli of CdS_xSe_{1-x} are calculated from the optimized volumes corresponding to the ground state energies. The lattice constants are shown against concentration x in Fig. 3. It is obvious from the plot that the lattice constant obey Vegard's law [32,33] and vary linearly with concentration x. In Table 1, the ground state energies, lattice constants and bulk moduli of both phases are compared with the previously reported experimental and theoretical results. From the table it is clear that our calculated values of the lattice constants and bulk moduli are closer to the experimental values as compared to other theoretical results.

4. Electronic properties

The binary compounds CdSe and CdS have direct band gaps of 1.8 and 2.56 eV in the zinc-blende structure and 1.8 and 2.63 eV in the wurtzite structure. The mixing of these two semiconducting compounds is interesting from the band gap engineering and optoelectronic point of view, because the alloy band gap energies cover the entire visible region of the electromagnetic spectrum (1.8–2.55 eV in zinc-blende and 1.8–2.63 eV in wurtzite). The calculated band structures of the ternary alloys of CdS_xSe_{1-x} in both phases are presented in Fig. 4a–f, which show that the band gaps for all the concentrations are direct and located at Γ symmetry line of the first brillouin zone. As direct band gap materials have fast decay time as compared to indirect band gap materials in the de-excitation process which is essential for the optically activeness of these materials in optoelectronic devices, and hence CdS_xSe_{1-x} ($0 \leqslant x \leqslant 1$) alloys are optically active in the visible region. The presently calculated band gap values of the alloy are compared with the reported results in Table 2 and also in Fig. 5. It is clear form table that our calculated values of the binary compounds are in

Table 1
Calculated ground state energy, E_0, lattice constants, a, c and bulk moduli, B, in the zinc-blende and wurtzite phases compared with the available literature.

X	Phase	Energy (*Ry*)	Lattice constant *a*, *c* (Å)			Bulk modulus (GPa)		
			Present	Exp.	Other Cal.	Present	Exp.	Other Cal.
0	B 3	−16044.151722	6.10	6.05[a]	6.21[c], 6.05[d]	64.62	53[a]	45.16[c], 65.12[d]
	B 4	−16044.112191	4.36,7.12	[4.3, 7.01][b]		57.96		
1/4	B 3	−60148.318372	6.05		6.15[c]	49.45		46.18[c]
	B 4	−60148.282280	4.31,7.06			46.53		
1/2	B 3	−56086.242875	5.99		6.08[c]	54.30		48.08[c]
	B 4	−56086.222740	4.28, 6.99			46.08		
3/4	B 3	−52024.164685	5.92		6.02[c]	57.31		50.93[c]
	B 4	−52024.170826	4.25,6.91			49.70		
1	B 3	−11984.082851	5.836	5.82[a]	5.95[c], 5.81[d]	72.27	62[a]	56.84[c], 72.42[d]
	B 4	−11984.113195	4.2,6.82	4.14, 6.72][b]		65.63		

[a] Ref. [34].
[b] Ref. [35].
[c] Ref. [28].
[d] Ref. [36].

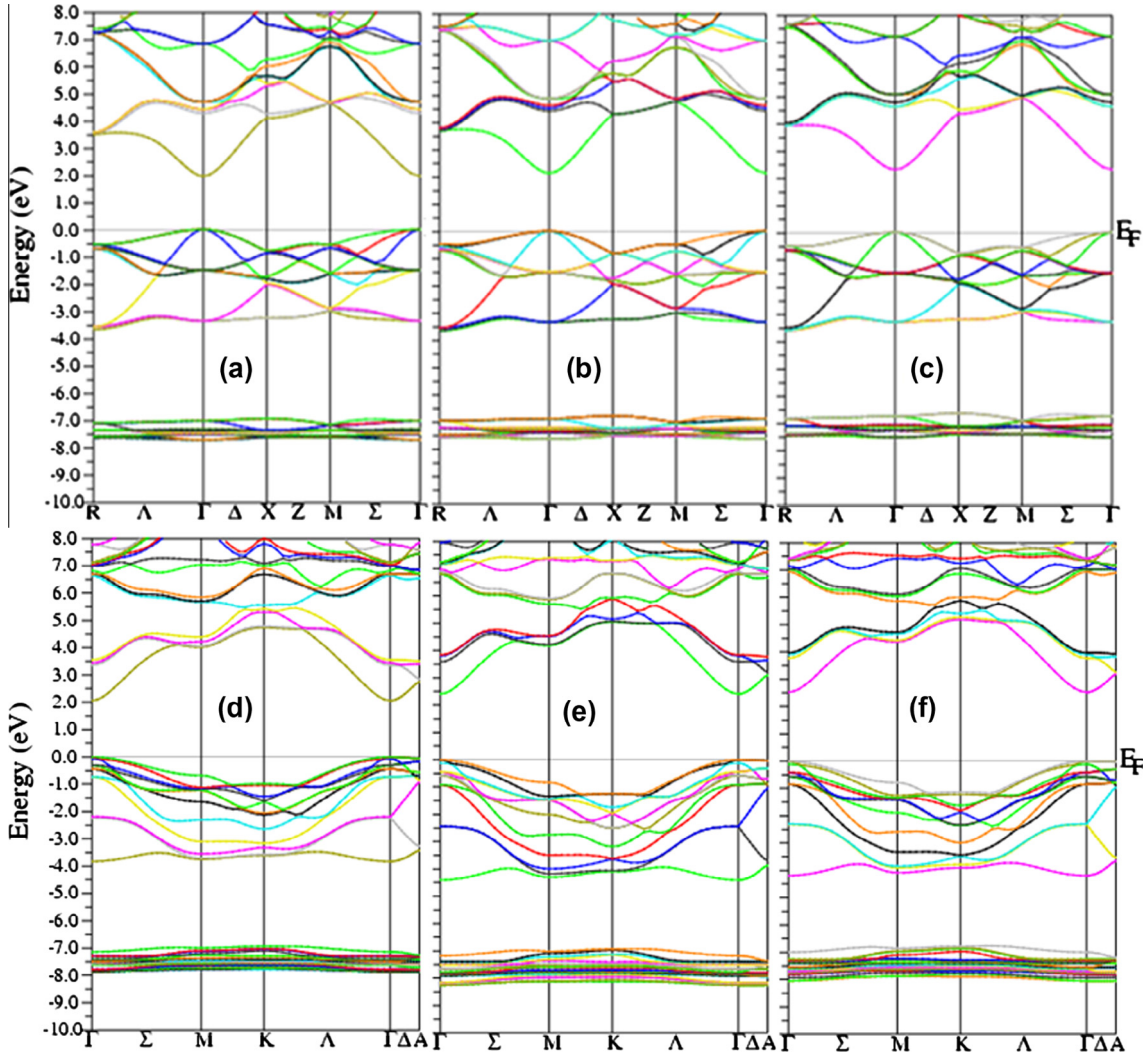

Fig. 4. Band gap energies of (a) $CdS_{0.25}Se_{0.75}$, (b) $CdS_{0.50}Se_{0.50}$, (c) $CdS_{0.75}Se_{0.25}$ in the zinc-blende and (d) $CdS_{0.25}Se_{0.75}$, (e) $CdS_{0.50}Se_{0.50}$, (f) $CdS_{0.75}Se_{0.25}$ in wurtzite phases.

Table 2
Calculated band gap energies (eV) in the zinc-blende and wurtzite structures compared with the available literature.

X	Zinc-blende (B3)			Wurtzite (B4)		
	Exp.	Theoretical		Exp.	Theoretical	
		Present	Other		Present	Other
0	1.82[e], 1.90[f]	1.80	1.20[c], 2.01[g], 1.89[h]	1.83[f]	1.80	1.91[g]
1/4		2.00	1.33[c]		2.05	
1/2		2.15	1.48[c]		2.40	
3/4		2.39	1.64[c]		2.50	
1	2.55[f]	2.56	1.8[c], 2.83[g], 2.66[h]	2.60[f]	2.63	2.79[g]

[c] Ref. [28].
[e] Ref. [22].
[f] Ref. [37].
[g] Ref. [38].
[h] Ref. [11].

agreement with the experimentally measured values, while the other available theoretical results are severely underestimated. The calculated band gap energies of CdS_xSe_{1-x} are plotted against the concentration x and compared with the reported experimental results [21] in Fig. 5. The results show that the alloy band gap energy varies linearly with concentration x in the zinc-blende phase with a negligible downward bowing parameter $b = 0.034$ eV, as given in Eq. (1). The wurtzite phase has upward bowing of 0.56 eV

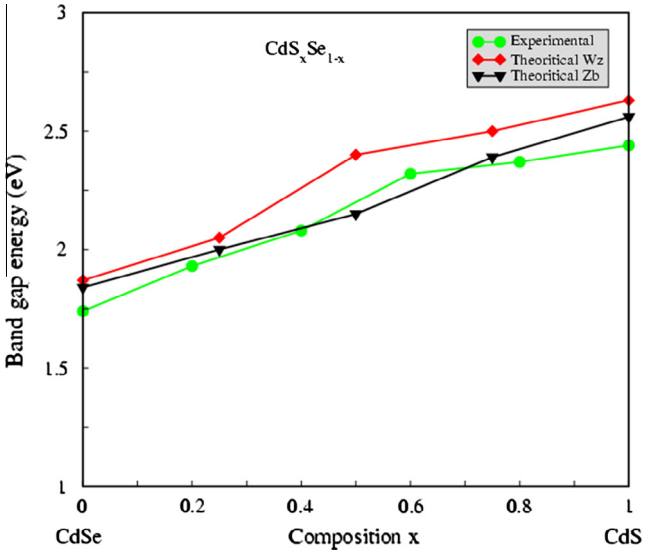

Fig. 5. Band gap energies as function of composition x in zinc-blende and wurtzite phases.

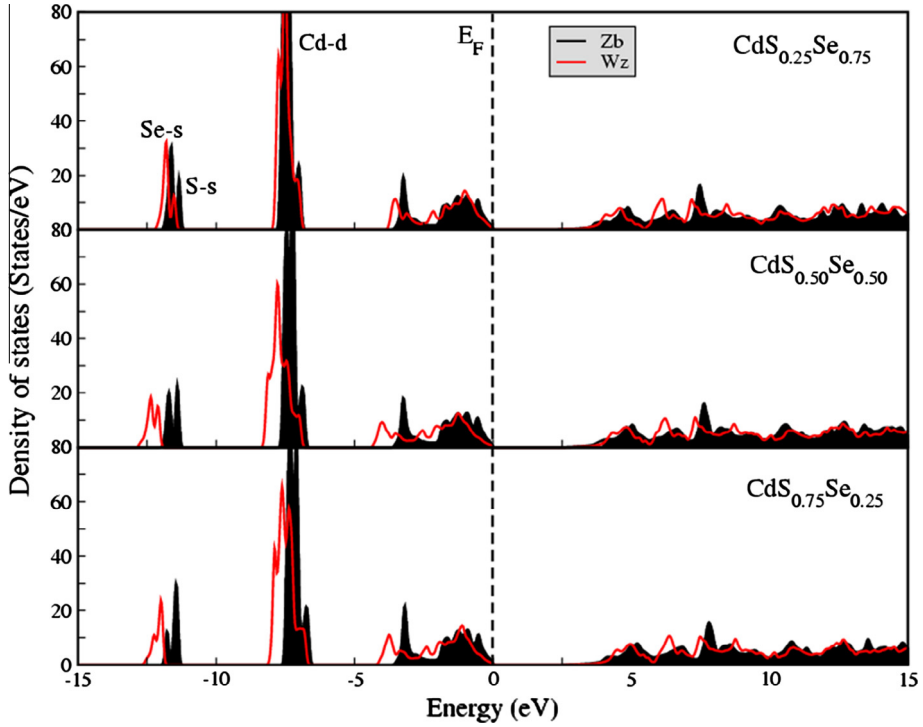

Fig. 6. Total density of states (DOSs) of CdS_xSe_{1-x} in zinc-blende and wurtzite phases.

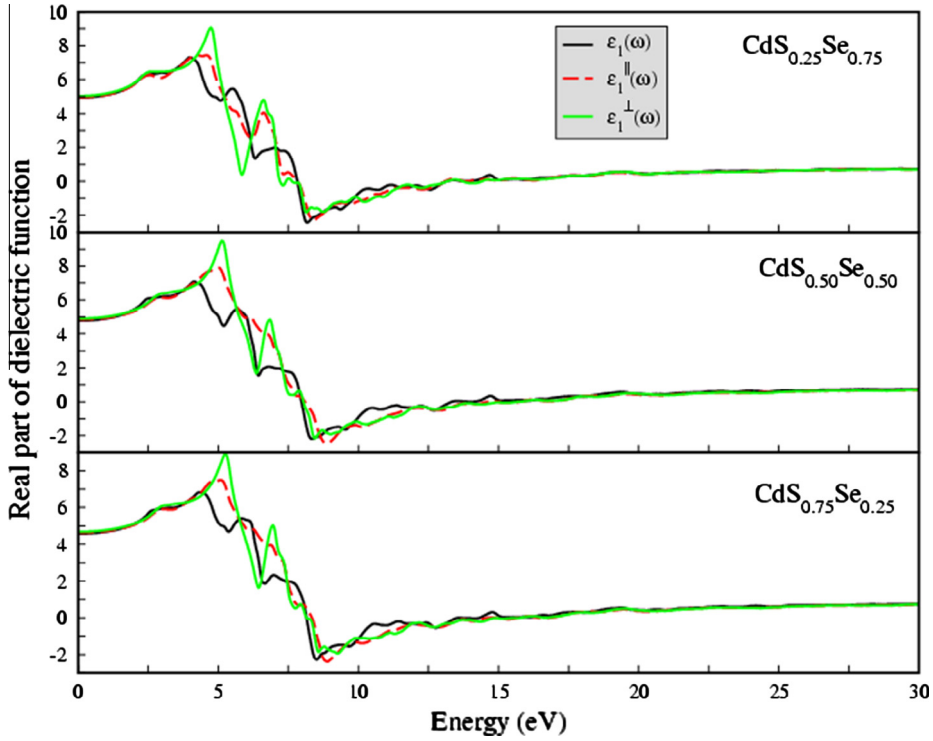

Fig. 7. Frequency dependent real part of dielectric function in zinc-blende and wurtzite phases.

with the increasing concentration *x*, as can be seen from the negative sign of the quadratic coefficient of bowing parameter b in Eq. (2) which is in agreement with the experimental work of Kumar and Sharma [21]. The present results, as given in Table 2, are quantitatively in good agreement with the experimental results, but appear slightly overestimated than the experimental results [21], as illustrated in Fig. 5. This may be because of the technique followed by the researcher in Ref. [21], because the band gap values for the binary compounds have discrepancy with other experimental results [22,37].

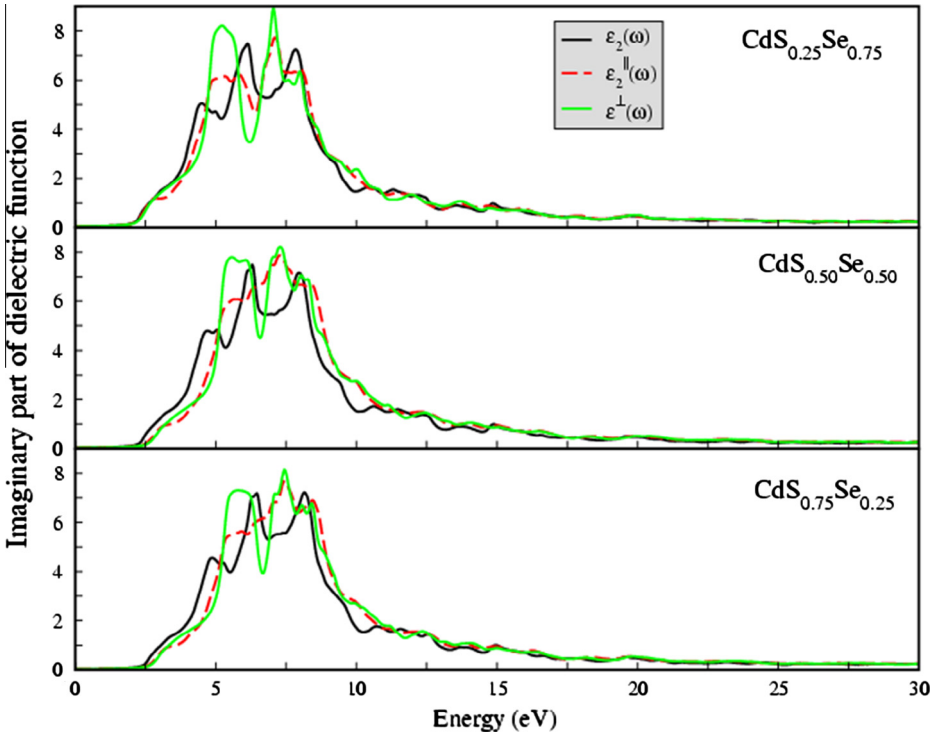

Fig. 8. Frequency dependent imaginary part of dielectric function in zinc-blende and wurtzite phases.

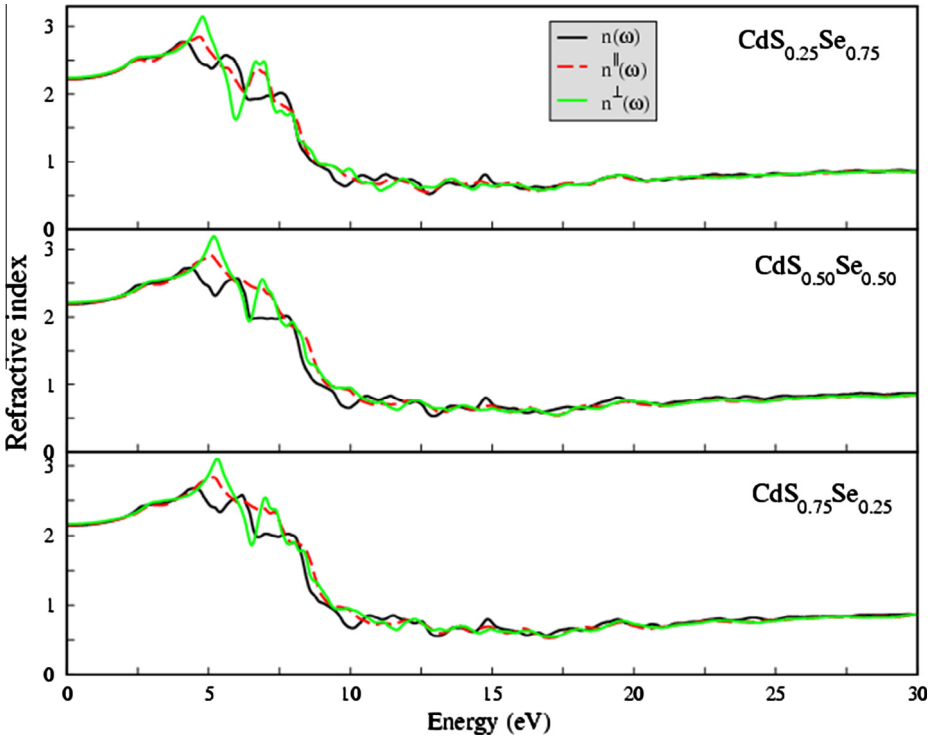

Fig. 9. Frequency dependent refractive index in zinc-blende and wurtzite phases.

$$\text{Zincblende} \Rightarrow E_g = 1.80 + 0.73x + 0.034x^2 \quad (1)$$

$$\text{Wurtzite} \Rightarrow E_g = 1.78 + 1.40x - 0.56x^2 \quad (2)$$

Density of states (DOSs) provides information about the location of different energy orbitals and also the bonding nature of the materials. The calculated DOS for CdS_xSe_{1-x} in both phases are plotted in Fig. 6. The bottom (lower) of the valence band consists of two peaks; the first is due to the Se-s and the second is due to the S-s states. The peaks at the intermediate of the valence band at energy around −7 eV is dominated by Cd-d state. In first-principle calculations this d-orbital plays vital role in determining the electronic band structures and chemical bonding. The previous approximations (LDA and GGA) used to approximate the exchange

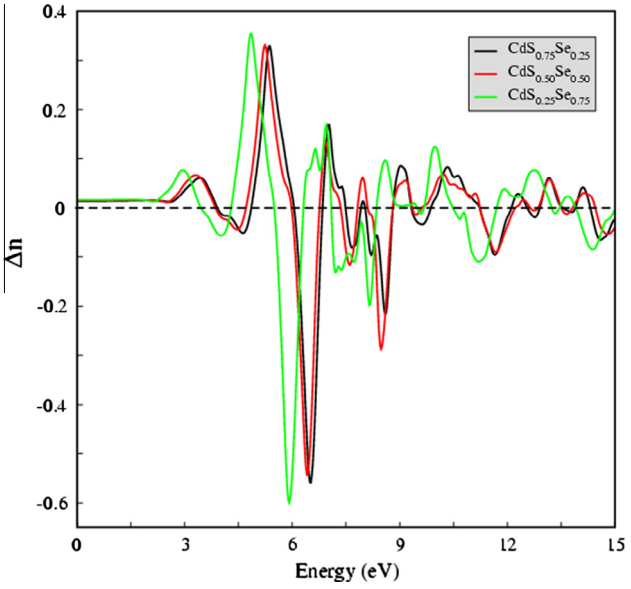

Fig. 10. Birefringence of wurtzite phases.

and correlation energies fail to locate the exact location of d-orbital and hence they overestimated the overlapping between the chalcogen-p and Cd-d state which caused severe underestimation of band gaps in the strongly correlated electron systems. The upper part of the valence band near the Fermi level is contributed by Cd-s and chalcogen-p states, while the lower conduction band is contributed by Cd-s and chalcogen-p states. As the concentration of S increases in CdSSe the ionic nature of the chemical bond increases which results in the expansion of the band gap.

5. Optical properties and birefringence

The band gap energies of CdS_xSe_{1-x} $(0 \leqslant x \leqslant 1)$ vary in the range 1.8−2.55 eV, which provides an appropriate opportunity to use the band gap as an adjustable parameter for the design of a desirable optoelectronic device working in the visible region of the electromagnetic spectrum. Depending upon the need and requirement of a particular application, any desired band gap between 1.8 and 2.55 eV can be achieved. As the tunable energy gap occurs in the visible range, therefore the optical properties of the alloys are also calculated.

The real parts of the complex dielectric function $\varepsilon_1(\omega)$ for CdS_xSe_{1-x} $(0 \leqslant x \leqslant 1)$ in both phases are calculated and presented in Fig. 7. The figure clearly shows the anisotropic nature of the compound in hexagonal structure. In hexagonal anisotropic materials the incident electromagnetic radiation decompose in to two components, the ordinary $\varepsilon_1^{\parallel}(\omega)$ and the extra ordinary $\varepsilon_1^{\perp}(\omega)$, corresponding to electric field perpendicular and parallel to *c*-axis. At low and high frequencies the material has similar behavior in both zinc-blende and wurtzite phases, while in the intermediate energy range (near the band edge and interband transitions) not only the phases show their significance but also anisotropy is observed in the wurtzite phase. The static dielectric function decreases with the increase in *x*, this decrease is due to the increase in the band gap of the alloy (1.8−2.5 eV). It is clear from the figure that with the increase in photon energy the real part of dielectric function also increases until a hump, which corresponds to fundamental band edge. After these humps the real part of dielectric function increase further and reaches the peak values. The maximum peak is due to R^v–R^c interband transition in the zinc-blende and Γ^{v}–Γ^{c} transition in the wurtzite structure. After the peak value it decreases rapidly.

The imaginary part of the complex dielectric function $\varepsilon_2(\omega)$ is calculated in the energy range 0−30 eV, plotted in Fig. 8. The

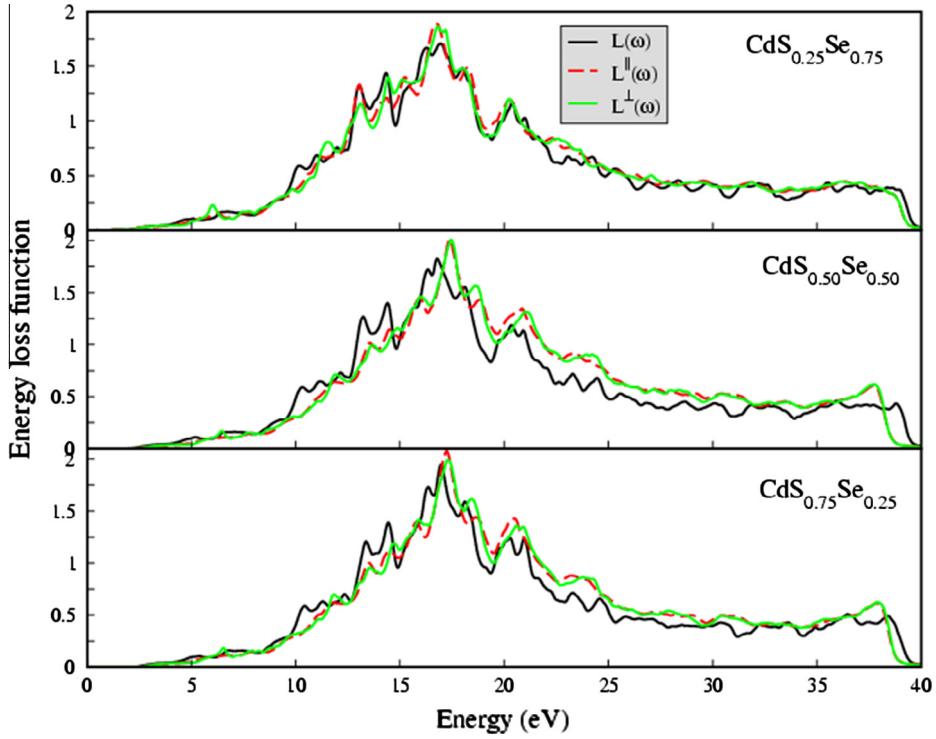

Fig. 11. Frequency dependent energy loss function (ELS) in zinc-blende and wurtzite phases.

anisotropy in the wurtzite phase can be vividly observed in the imaginary part of the dielectric function. From the offset points the optical gaps can be calculated. The spectra show that the compound has high absorption in the energy range 2.5−10 eV. In the absorption region for the wurtzite phase the parallel component $\varepsilon_2^{\parallel}(\omega)$ has a single peak, while the perpendicular $\varepsilon_2^{\perp}(\omega)$ has a shoulder and a peak, whereas in the zinc-blende the imaginary part of the dielectric function has two peaks. The variations in the absorption spectrum for different concentration of S make the compound suitable for optical device technology operating in the visible part of the spectrum.

The calculated refractive index for CdS_xSe_{1-x} ($0 \leqslant x \leqslant 1$) in the energy range 0−30 eV is plotted in Fig. 9. From the figure it is clear that zero frequency refractive index decreases with the increasing concentration of S. The maximum peak shifts towards higher energy levels as the concentration of S is increased. The refractive index has similar pattern as the real part of dielectric function. At higher energies than 8 eV the refractive index becomes less than unity ($c/v < 1$), which means that the material can no longer act as a transparent material.

In the wurtzite phase we have two optical axes, ordinary $n^{\parallel}(\omega)$ and extraordinary $n^{\perp}(\omega)$ components. Birefringence Δn ($\Delta n = n_e - n_o$) is given in Fig. 10. At low energy levels we have positive birefringence, mean that fast rays travel parallel to the applied field and slow rays travel in the z-axis, means that the extra ordinary component have greater dispersion. While for higher incident photon frequency, the z-axis have fast radiations and the ordinary component have large dispersion. Birefringence is extensively used in optical devices, such as color filters, light modulators, liquid crystal displays, wave plates, optical axis gratings, etc. Birefringent filters are used to spread the image in one direction in electronic cameras, which increases the spot-size. This is necessary for proper working of all television and electronic film cameras.

The electron energy loss spectra for CdS_xSe_{1-x} ($0 \leqslant x \leqslant 1$) are also calculated to investigate the interaction of incident photons with the compound, plotted in Fig. 11. The figure shows that CdS_xSe_{1-x} has isotropic nature, because of the less difference in the ordinary and extraordinary parts of the energy loss function. The maximum peak value appears at 16.78, 17.41 and 17.24 eV energies for $CdS_{0.25}Se_{0.75}$, $CdS_{0.50}Se_{0.50}$ and $CdS_{0.75}Se_{0.25}$, respectively. These peaks in the energy loss spectrum correspond to plasma resonance and the corresponding frequencies are called plasma frequencies. Above these peaks the materials exhibit metallic behavior, whereas below these peaks they behave like dielectrics.

6. Conclusions

First principle calculations of CdS_xSe_{1-x} ($0 \leqslant x \leqslant 1$) are carried out using FP-LAPW method. The structure parameters like lattice constants and bulk moduli are optimized using GGA. The binary compounds CdSe and CdS crystallize in the zinc-blende as well as wurtzite phases. The crystal phase of the ternary compound CdS_xSe_{1-x} transforms from the zinc-blende to wurtzite at $x = 68\%$. The electronic and optical properties are calculated using the mBJ exchange potential. The alloy has direct band gap nature for the whole range of concentration in both zinc-blende and wurtzite phases. The band gaps vary from 1.8 to 2.56 eV covering the entire range of the electromagnetic spectrum in the visible range. The calculated optical properties conforms considerable anisotropy in the wurtzite phase. Furthermore the birefringence is also calculated, which shows that the ordinary optical axis has fast light for lower incident photon frequency while larger dispersion for higher photon frequency.

References

[1] D.C. Kundalia, S.B. Ogale, S.E. Lofland, S. Dhar, C.J. Metting, S.R. Shinde, Z. Ma, B. Varughese, K.V. Ramanujachary, L. Salamanca-Riba, T. Venkatesan, Nat. Mater. 3 (2004) 709.
[2] Z. Wang, L.L. Daemen, Y. Zhao, C.S. Zha, R.T. Downs, X. Wang, Z.L. Wang, R.J. Hemley, Nat. Mater. 4 (2005) 922.
[3] D.A. Bussian, S.A. Crooker, M. Yin, M. Brynda, A.L. Efros, V.I. Klimov, Nat. Mater. 8 (2009) 35.
[4] J. Lu, Y. Dai, M. Guo, W. Wei, Y. Ma, S. Han, B. Huang, ChemPhysChem 13 (2012) 147.
[5] W. Wei, Y. Dai, K. Yang, M. Guo, B. Huang, J. Phys. Chem. C 112 (2008) 15915.
[6] F. Tran, P. Blaha, Phys. Rev. Lett. 102 (2009) 226401.
[7] I. Khan, I. Ahmad, H.A.R. Aliabad, M. Maqbool, J. App. Phys. 112 (2012) 073104.
[8] I. Khan, I. Ahmad, Int. J. Quantum Chem. 113 (2013) 1285.
[9] I. Khan, A. Afaq, H.A.R. Aliabad, I. Ahmad, Compos. Mater. Sci. 61 (2012) 278.
[10] I. Khan, I. Ahmad, D. Zhang, H.A.R. Aliabad, S.J. Asadabadi, Phys. Chem. Solids 74 (2013) 181.
[11] H.H. Gurel, O. Akinci, H. Unlu, Superlattices Microstruct. 51 (2012) 725.
[12] M. Elisa, C. Vasiliu, J. Striber, D. Radua, J.H. Trodahlb, M. Dalley, J. Optoelectron. Adv. Mater. 8 (2006) 811.
[13] M. Ivanda, T. Bischof, G. Lermann, A. Materny, W. Kiefer, J. Appl. Phys. 82 (1997) 3116.
[14] R.K. Jain, R.C. Lind, J. Opt. Soc. Am. 73 (1983) 647.
[15] N.F. Borrelli, D.W. Hall, H.J. Holland, D.W. Smith, J. Appl. Phys. 61 (1987) 5399.
[16] G.I. Stegeman, C.T. Seaton, J. Appl. Phys. 58 (1985) R57.
[17] G.P. Banfi, V. Degiorgio, H.M. Tan, J. Opt. Soc. Am. B 12 (1995) 621.
[18] C. Sifuentes, Y. Barmenkov, A. Strodumov, V. Filipov, A. Lipovskii, Opt. Eng. 39 (2000) 2182.
[19] J. Wang, B. Huang, Z. Wang, P. Wang, H. Cheng, Z. Zheng, X. Qin, X. Zhang, Y. Dai, M.H. Whangbo, J. Mater. Chem. 21 (2011) 4562.
[20] O.P. Agnihotri, A.K. Raturi, Thin Solid Films 108 (1983) 313.
[21] V. Kumar, T.P. Sharma, J. Phys. Chem. Solids 59 (1998) 1321.
[22] C.W. White, A. Meldrum, J.D. Budai, S.P. Withrow, E. Sonder, R.A. Zuhr, D.M. Hembree Jr., M. Wu, D.O. Henderson, Nucl. Instrum. Methods Phys. Res., Sect. B 148 (1999) 991.
[23] A. Pan, H. Yang, R. Yu, B. Zou, Nanotechnology 17 (2006) 1083.
[24] R.C. Kainthla, D.K. Pandya, K.L. Chopra, J. Electrochem. Soc. 129 (1982) 99.
[25] Y. Liang, L. Zhai, X. Zhao, D. Xu, J. Phys. Chem. B 109 (2005) 7120.
[26] Y.L. Kim, J.H. Jung, K.H. Kim, H.S. Yoon, M.S. Song, S.H. Bae, Y. Kim, Nanotechnology 20 (2009) 095605.
[27] R.B. Liu, J.H. Cao, Z.A. Li, Q. Wang, Q.L. Zhang, P.B. He, B.S. Zou, A.L. Pan, J. Phys.: Condens. Matter 21 (2009) 375302.
[28] S. Ouendadji, S. Ghemid, H. Meradji, F.E.H. Hassan, Compos. Mater. Sci. 48 (2010) 206.
[29] P. Blaha, K. Schwarz, G.K.H. Madsen, D. Kvasnicka, J. Luitz, WIEN2k, An augmented plane wave plus local orbitals program for calculating crystal properties, Vienna University of Technology, Vienna, Austria, 2001.
[30] R. Thangavel, M. Rajagopalan, J. Kumar, Physica B 403 (2008) 1824.
[31] F.D. Murnaghan, Proc. Natl. Acad. Sci. USA 30 (1944) 244.
[32] L. Vegard, Z. Phys. 5 (1921) 17.
[33] L. Vegard, Z. Cryst. 67 (1928) 239.
[34] O. Madelung, M. Schlz, H. Weiss, Landolt-Borstein (Eds.), Numerical Data and Functional Relationships in Science and Technology, vol. 17, Springer, Berlin, 1982.
[35] U. Hotje, C. Rose, M. Binnewies, Solid State Sci. 5 (2003) 1259.
[36] E. Deligoz, K. Colakoglu, Y. Ciftci, Physica B 373 (2006) 124.
[37] K.-H. Hellwege, O. Madelung, Landolt-Bornstein, Numerical Data and Functional Relationships in Science and Technology, 17a and 22a, Springer, New York, 1982.
[38] O. Zakharov, A. Rubio, X. Blase, Marvin L. Cohen, S.G. Louie, Phys. Rev. B 50 (1994) 10780.